Chapter 4
Adaptive Design for Reference Velocity Recovery: Parameterization Approach

4.1 Introduction

The designs in Sections 3.3 and 3.5 restrict the reference velocity $v(t)$ to be constant or periodically time-varying. In this section, we present adaptive designs that are applicable to any time-varying, uniformly bounded and C^1 reference velocity $v(t)$ that can be parameterized as

$$v(t) = \sum_{j=1}^{r} \phi^j(t)\theta^j = (\Phi(t)^T \otimes I_p)\theta \tag{4.1}$$

where $\phi^j(t) \in \mathbb{R}$, $j = 1, \cdots, r$ are basis functions available to each agent, $\theta^j \in \mathbb{R}^p$ are column vectors available only to the leader,

$$\Phi(t) = [\phi^1(t), \cdots, \phi^r(t)]^T \tag{4.2}$$

and

$$\theta = [(\theta^1)^T, \cdots, (\theta^r)^T]^T. \tag{4.3}$$

We let agent i, $i = 2, \cdots, N$, estimate the unknown θ^j by $\hat{\theta}_i^j$, and construct $\hat{v}_i(t)$ from

$$\hat{v}_i(t) = \sum_{j=1}^{r} \phi^j(t)\hat{\theta}_i^j = (\Phi(t)^T \otimes I_p)\hat{\theta}_i \quad i = 2, \cdots, N, \tag{4.4}$$

where

$$\hat{\theta}_i = [(\hat{\theta}_i^1)^T, \cdots, (\hat{\theta}_i^r)^T]^T. \tag{4.5}$$

In the following sections, we first develop a basic adaptive design with which agent i updates its estimate $\hat{\theta}_i$, $i = 2, \cdots, N$. Like the design in Section 3.3, this basic adaptive design recovers objective A2 as well as guaranteeing objective A1 in some special cases, such as, the agreement problem. To ensure objective A1 when the basic adaptive design fails, we then modify the basic adaptive design in a similar

H. Bai et al., *Cooperative Control Design: A Systematic, Passivity-Based Approach*, Communications and Control Engineering 89, DOI 10.1007/978-1-4614-0014-1_4,

fashion to Section 3.5 and obtain the augmented adaptive design. We next apply the adaptive design result to an extremum seeking example. In this example, a group leader autonomously determines the Newton direction towards the extremum by sampling a field distribution and parameterizes the group reference velocity according to the Newton direction. The other agents then estimate this reference velocity using the basic adaptive design and reconstruct the desired formation during extremum seeking. Before proceeding to these results, we first compare the parameterization approach and the internal model approach.

In the parameterization approach, the availability of the basis functions to each agent is similar to Assumption 1 in the internal model approach, where the $\bar{A}$ matrix is available to each agent. The use of the basis functions $\phi^j(t)$ removes the restriction in the internal model approach that $v(t)$ be constant or periodic. The basis functions may then be used to shape the transient of the reference velocity profile. However, since $\phi^j(t)$'s are time-dependent, the agents need to have synchronized clocks to implement this parameterization approach. The next example compares the number of the internal states used for estimating periodic reference velocity in these two approaches.

Example 4.1. We consider a scalar reference velocity $v(t)$, parameterized by

$$v(t) = \sum_{i=1}^{r_1} (a_i \sin(w_i t) + b_i \cos(w_i t)). \tag{4.6}$$

Note that $v(t)$ in (4.6) is already parameterized by the basis functions $\sin(w_i t)$ and $\cos(w_i t)$, $i = 1, \cdots, r_1$. Therefore, the total number of unknown parameters that parameterizes this $v(t)$ is $2r_1$, which means that for the parameterization approach, each agent (except the leader) needs to update $2r_1$ internal states to estimate these unknown parameters.

In the internal model approach, we choose $\bar{A}$ in (3.15) as

$$\bar{A} = \text{diag}\left\{ \begin{pmatrix} 0 & -w_1 \\ w_1 & 0 \end{pmatrix}, \cdots, \begin{pmatrix} 0 & -w_{r_1} \\ w_{r_1} & 0 \end{pmatrix} \right\} \tag{4.7}$$

which implies that the dimension of ϖ_i in (3.29) is $2r_1$. This means that each agent (except the leader) also maintains $2r_1$ internal states to estimate the reference velocity. Thus, in estimating generic periodic reference velocities, both the parameterization approach and the internal model approach use the same number of internal states.

In some special cases, however, the parameterization approach may require less internal states. For example, if in (4.6) $b_i = 0$, $i = 1, \cdots, r_1$, then the parameterization approach only requires r_1 internal states which estimate all a_i's while the internal model approach still requires $\bar{A}$ to be the same as (4.7) and the dimension of ϖ_i to be $2r_1$. □

4.2 The Basic Design

We choose the update law for the parameter $\hat{\theta}_i$ in (4.4) as

$$\dot{\hat{\theta}}_i = \Lambda_i(\Phi(t) \otimes I_p)u_i \tag{4.8}$$

in which $\Lambda_i = \Lambda_i^T > 0$ and u_i is as in (2.23). As proven in Theorem 4.1 below, the basic adaptive design (3.23), (3.24), and (4.8) guarantees convergence to the desired target sets (objective A2). Whether objective A1 is achieved or not depends on the convergence of $\hat{\theta}_i$ to θ, which will be studied in Section 4.3. When $\hat{\theta}_i$ converges to θ, $v(t)$ is recovered with the adaptive design and, thus, object A1 is also achieved.

Theorem 4.1. *Consider the coordination laws in (3.23), (3.24), (4.4) and (4.8) where $v(t)$ is uniformly bounded and piecewise continuous, parameterized as (4.1) in which $\phi^j(t)$, $j = 1,\cdots,r$ are uniformly bounded, and $\mathscr{H}_i$, $i = 1,\cdots,N$, and ψ_k, $k = 1,\cdots,\ell$ are designed as in (2.11)-(2.15) and (2.27)-(2.31), respectively. Then, the set*

$$\mathscr{E}^* = \left\{(z,\xi,\hat{\theta}) |\ \xi = 0,\ (D \otimes I_p)\psi(z) = 0 \text{ and } z \in \mathscr{R}(D^T \otimes I_p),\ \hat{\theta} = \theta^*\right\} \tag{4.9}$$

is stable, where $\hat{\theta} = [\hat{\theta}_2^T,\cdots,\hat{\theta}_N^T]^T$ and $\theta^* = 1_{N-1} \otimes \theta$. All trajectories $(z(t),\xi(t),\hat{\theta}(t))$ starting in $\mathscr{G} \times \mathbb{R}^{pr(N-1)}$ are bounded and converge to the set $\mathscr{E} \times \mathbb{R}^{pr(N-1)}$, where $\mathscr{E}$ and $\mathscr{G}$ are as in (2.33) and (2.37). Moreover, when Property 2.1 holds, all trajectories $(z(t),\xi(t),\hat{\theta}(t))$ starting in $\mathscr{G} \times \mathbb{R}^{pr(N-1)}$ converge to the set $\mathscr{A} \times \mathbb{R}^{pr(N-1)}$, where $\mathscr{A}$ is as in (2.36). □

To obtain the closed-loop structure of the basic adaptive design, we denote by $\tilde{\theta}_i$ the error variable

$$\tilde{\theta}_i = \hat{\theta}_i - \theta \quad i = 2,\cdots,N, \tag{4.10}$$

and note from (4.8) that

$$\dot{\tilde{\theta}}_i = \Lambda_i(\Phi(t) \otimes I_p)u_i. \tag{4.11}$$

Using (4.1) and (4.4), we get

$$\tilde{v}_i = \hat{v}_i - v(t) = (\Phi(t)^T \otimes I_p)\tilde{\theta}_i, \quad i = 2,\cdots,N. \tag{4.12}$$

We set $\tilde{\theta}_1 \equiv 0$ and $\tilde{v}_1 \equiv 0$, and define

$$\tilde{\theta} = [\tilde{\theta}_1^T,\tilde{\theta}_2^T,\cdots,\tilde{\theta}_N^T]^T \tag{4.13}$$

and

$$\tilde{v} = (I_N \otimes \Phi^T(t) \otimes I_p)\tilde{\theta} = [\tilde{v}_1^T,\cdots,\tilde{v}_N^T]^T. \tag{4.14}$$

The closed-loop structure of the basic adaptive design is then shown in Fig. 4.1.

We now give a passivity interpretation of the basic adaptive design. Because the single integrator is passive and because the feedback path from u to $\tilde{v}$ exhibits the same structure as Structure 1, we obtain the passivity from u to $\tilde{v}$. We then conclude

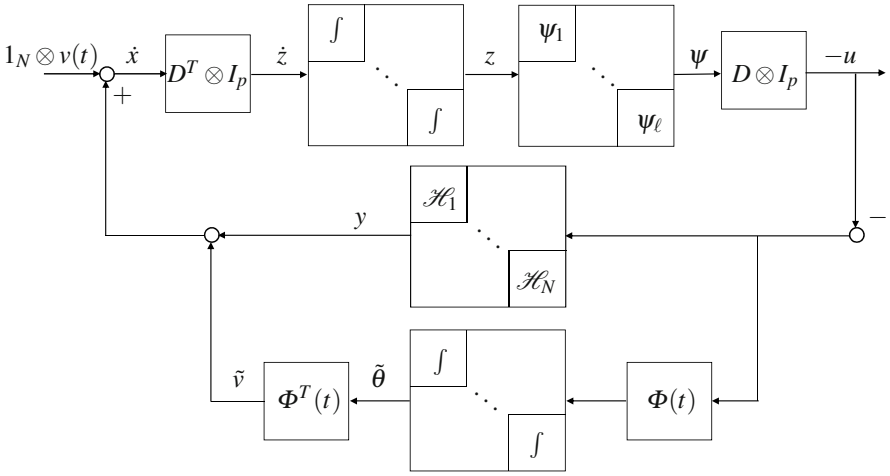

Fig. 4.1 The closed-loop structure of the basic adaptive design. The appearance of $\Phi(t)$ and its transpose before and after the integrator implies the passivity from u to $\tilde{v}$. The closed-loop stability follows from the interconnection of the passive feedforward path and the passive feedback paths.

from the passivity result *ii*) in Theorem 2.1 and Structure 2 that the feedback path is passive from u to $y+\tilde{v}$. As proven in Theorem 2.1, the feedforward path is also passive. Therefore, the closed-loop stability follows from Structure 3. The detailed proof is given below.

Proof. To prove the stability of the closed-loop system described by the adaptive design (2.11), (3.55) and (4.11), we exploit the passivity properties of the interconnected systems and consider $V_f(z)$ and $V_b(\xi)$ in (2.35) and

$$V_a(\tilde{\theta}) = \frac{1}{2}\sum_{i=2}^{N} \tilde{\theta}_i^T \Lambda_i^{-1} \tilde{\theta}_i, \tag{4.15}$$

which are the storage functions for the three paths in Fig. 4.1. In particular, the time derivatives of $V_f(z)$ and $V_b(\xi)$ are the same as (3.56) and (2.40).

Using (4.11), we obtain

$$\begin{aligned}
\dot{V}_a &= \sum_{i=2}^{N} \tilde{\theta}_i^T \Lambda_i^{-1} \dot{\tilde{\theta}}_i \\
&= \sum_{i=2}^{N} \tilde{\theta}_i^T \Lambda_i^{-1} \Lambda_i (\Phi(t) \otimes I_p) u_i \\
&= \sum_{i=2}^{N} \tilde{\theta}_i^T (\Phi(t) \otimes I_p) u_i \\
&= u^T \tilde{v}.
\end{aligned} \tag{4.16}$$

From (2.40), (3.56) and (4.16), the Lyapunov function

$$V(z,\xi,\tilde{\theta}) = V_f(z) + V_b(\xi) + V_a(\tilde{\theta}) \tag{4.17}$$

yields the negative semidefinite derivative

$$\dot{V} \leq -\sum_{i\in\mathscr{I}}^{N} W_i(\xi_i) - \sum_{i\notin\mathscr{I}} u_i^T y_i \leq 0 \tag{4.18}$$

which implies that all the trajectories $(z(t),\xi(t),\tilde{\theta}(t))$ are bounded. We further conclude from Theorem B.5 in Appendix B.3 that $\xi_i \to 0$, $\forall i \in \mathscr{I}$ and that $u_i \to 0$, $\forall i \notin \mathscr{I}$. We next show that $u_i \to 0$, $\forall i \in \mathscr{I}$. To this end we note that

$$\ddot{\xi}_i = \frac{\partial f_i}{\partial u_i}\dot{u}_i + \frac{\partial f_i}{\partial \xi}\dot{\xi}_i \tag{4.19}$$

is continuous and uniformly bounded because $\dot{u}$ and $\dot{\xi}$ are continuous functions of the bounded signals $(z(t),\xi(t),\tilde{\theta}(t),\Phi(t))$ and because $f_i(\cdot,\cdot)$ is C^1. Since $\xi_i \to 0$ and $\ddot{\xi}_i$ is continuous and bounded, it follows from Theorem B.4 in Appendix B.3 that $\dot{\xi}_i \to 0$, which, from (2.11) and (2.12), guarantees $u_i \to 0$.

Finally, we note that $u \to 0$ implies from (2.26) that $\psi(z)$ converges to the null space $\mathscr{N}(D\otimes I_p)$. This, in turn, implies that the trajectories $(z(t),\xi(t),\hat{\theta}(t))$ starting in $\mathscr{G}\times\mathbb{R}^{pr(N-1)}$ converge to the set $\mathscr{E}\times\mathbb{R}^{pr(N-1)}$, where $\mathscr{E}$ and $\mathscr{G}$ are as in (2.33) and (2.37). Moreover, when Property 2.1 holds, all trajectories converge to the set $\mathscr{A}\times\mathbb{R}^{pr(N-1)}$, where $\mathscr{A}$ is as in (2.36). □

4.3 Parameter Convergence

Parameter convergence is essential for recovering objective A1 in Section 2.2 because $\hat{\theta}_i \to \theta$ implies $|\hat{v}_i(t) - v(t)| \to 0$. In this section, we restrict our attention to the group agreement problem as a special case of the adaptive design and show that the parameter convergence is achieved. We note, however, that the convergence to the desired target set (objective A2) is guaranteed by Theorem 4.1 even without parameter convergence.

We assume that $P_k(z_k)$'s are positive definite and radially unbounded functions on $\mathscr{G}_k = \mathbb{R}^p$ such that (2.46) is satisfied and thus, Property 2.1 holds. We further assume that the passive feedback block $\mathscr{H}_i$ is in the control affine form

$$\dot{\xi}_i = f_i(\xi_i) + g_i(\xi_i)u_i \tag{4.20}$$

$$y_i = h_i(\xi_i) \tag{4.21}$$

where

$$h_i(0) = 0, \qquad f_i(0) = 0 \tag{4.22}$$

and that the regressor $\Phi(t)$ in (4.4) is *persistently exciting* (PE), which means that for all $t_o \geq 0$,

$$\int_{t_o}^{t_o+\delta} \Phi(t)\Phi(t)^T dt \geq \alpha I \tag{4.23}$$

with some constants $\delta > 0$ and $\alpha > 0$ that do not depend on t_o. This PE condition ensures the information richness of the time-varying signal $\Phi(t)$ throughout time, and guarantees parameter convergence:

Theorem 4.2. *In Theorem 4.1, suppose that the desired sets are $\mathscr{A}_k = \{0\}$, and that the passive feedback block is of the form (4.20)-(4.22). If $\Phi(t)$ satisfies the PE condition (4.23), then the origin of $(z, \xi, \tilde{\theta})$ is globally uniformly asymptotically stable. In particular, $\hat{\theta}_i \to \theta$, $i = 2, \cdots, N$ as $t \to \infty$.* □

Proof. To prove parameter convergence in this case, we use the Nested Matrosov Theorem reviewed in Appendix B.5. The first auxiliary function V_1 is the same as the Lyapunov function V in (4.17), which yields the negative semidefinite derivative in (4.18) and thus guarantees uniform global stability, that is,

$$\dot{V}_1 = \dot{V} \leq \sum_{i=1}^{N} -W_i(\xi_i) := Y_1 \leq 0. \tag{4.24}$$

The second auxiliary function is

$$V_2 = z^T (D \otimes I_p)^+ \Gamma y \tag{4.25}$$

where $(D \otimes I_p)^+$ denotes the pseudoinverse of $D \otimes I_p$ and

$$\Gamma = \text{diag}\{(L_{g_1} h_1(0))^{-1}, \cdots, (L_{g_N} h_N(0))^{-1}\}. \tag{4.26}$$

In particular $L_{g_i} h_i(0) := \frac{\partial h_i(\xi_i)}{\partial \xi_i}\big|_{\xi_i=0} g_i(0)$ is nonsingular and thus invertible because of the passivity of the ξ_i-subsystems in (4.20) and because of Proposition B.1 in Appendix B.4. The derivative of V_2 yields

$$\dot{V}_2 = z^T (D \otimes I_p)^+ \Gamma \dot{y} + \dot{z}^T (D \otimes I_p)^+ \Gamma y := Y_2 \tag{4.27}$$

where we claim that

$$Y_1 = 0 \quad \Rightarrow \quad Y_2 \leq 0. \tag{4.28}$$

To see this, note that $Y_1 = 0$ implies $\xi = 0$ and it follows from (4.22) that $y = 0$, which means that the second term in $\dot{V}_2$ vanishes. Because $\dot{y}_i = L_{g_i} h_i(0) u_i$ when $\xi = 0$, Y_2 becomes

$$Y_2 = z^T (D \otimes I_p)^+ u. \tag{4.29}$$

Substituting (2.26) and $z^T = x^T (D \otimes I_p)$ from (2.6), we obtain

$$\begin{aligned} Y_2 &= -x^T (D \otimes I_p)(D \otimes I_p)^+ (D \otimes I_p) \psi(z) \\ &= -x^T (D \otimes I_p) \psi(z) \end{aligned}$$

$$= -z^T \psi(z) \leq 0. \tag{4.30}$$

Next we introduce the auxiliary function

$$V_3 = -((D^T \otimes I_p)\tilde{v})^T z \tag{4.31}$$

where $\tilde{v}$ is defined in (4.14). Its derivative is

$$\dot{V}_3 = -((D^T \otimes I_p)\tilde{v})^T \dot{z} - ((D^T \otimes I_p)\dot{\tilde{v}})^T z := Y_3 \tag{4.32}$$

and we claim

$$Y_1 = 0,\ \ Y_2 = 0 \ \ \Rightarrow \ \ Y_3 = -\left\{(D^T \otimes I_p)\tilde{v}\right\}^T \left\{(D^T \otimes I_p)\tilde{v}\right\} \leq 0. \tag{4.33}$$

To show (4.33), we first note that $Y_2 = 0$ implies that $z^T \psi(z) = 0$ and thus $z = 0$ due to (2.46), which means that the second term in (4.32) vanishes. It follows from $Y_1 = 0$ that $\xi = 0$ and hence y is zero from (4.22). Therefore, $\dot{z}$ in (3.55) becomes $(D^T \otimes I_p)\tilde{v}$, which proves (4.33).

Finally, we define the auxiliary function

$$V_4 = -\tilde{\theta}^T S(t)\tilde{\theta} \tag{4.34}$$

$$S(t) := \int_t^\infty e^{(t-\tau)} F(\tau)F(\tau)^T d\tau \quad F(t) := I_N \otimes \Phi(t) \otimes I_p \tag{4.35}$$

where

$$S(t) \geq \int_t^{t+\delta} e^{(t-\tau)} F(\tau)F(\tau)^T d\tau \geq \alpha e^{-\delta} I \tag{4.36}$$

because of the PE property of $\Phi(t)$. Note that

$$\begin{aligned} \dot{S}(t) &= e^t \int_t^\infty e^{-\tau} F(\tau)F(\tau)^T d\tau + e^t \frac{d}{dt}\left\{\int_t^\infty e^{-\tau} F(\tau)F(\tau)^T d\tau\right\} \\ &= S(t) - F(t)F(t)^T. \end{aligned} \tag{4.37}$$

From (4.37), we obtain

$$\dot{V}_4 \leq -\tilde{\theta}^T S(t)\tilde{\theta} + \tilde{v}^T \tilde{v} - 2\tilde{\theta}^T S(t)\dot{\tilde{\theta}} := Y_4 \tag{4.38}$$

and claim

$$Y_2 = 0,\ Y_3 = 0 \ \ \Rightarrow \ \ Y_4 = -\alpha e^{-\delta} |\tilde{\theta}|^2 \leq 0 \tag{4.39}$$

because the second and third terms in (4.38) vanish when $Y_2 = 0$ and $Y_3 = 0$. Indeed, $Y_3 = 0$ leads to $(D^T \otimes I_p)\tilde{v}(t) = 0$, which indicates that $\tilde{v}(t)$ lies in $\mathcal{N}(D^T \otimes I_p)$. Recall that $\mathcal{N}(D^T \otimes I_p) = 1_N \otimes c$, $c \in \mathbb{R}^p$ and $\tilde{v}_1 \equiv 0_p$. Therefore, it follows that $\tilde{v}(t) = 0$, which means that the second term in Y_4 (4.38) is zero. Likewise, from (2.46), $Y_2 = 0$ results in $z = 0$, which means z belongs to the desired set $\mathcal{A}$ and thus $\psi(z)$ and u are zero. It follows that $\dot{\tilde{\theta}} = 0$ from (4.11), which shows that the third term in Y_4 vanishes.

Because $Y_i = 0$, $i = 1,2,3,4$, imply $(\xi, z, \tilde{\theta}) = 0$ and we conclude from the Nested Matrosov Theorem in Appendix B.5 that the origin is globally uniformly asymptotically stable. Note that $\tilde{\theta} \to 0$ implies $\hat{\theta}_i \to \theta$, $i = 2, \cdots, N$. □

4.4 The Augmented Design

Like the design in Section 3.3, the basic adaptive design in Section 4.2 ensures tracking of reference velocity (objective A1) only in special cases, such as the agreement problem studied in the previous section. To guarantee objective A1 when the basic adaptive design fails, we employ the augmented design (3.68) in the update law (4.8). The augmented design recovers the stability result of Theorem 2.1 and achieves tracking of the reference velocity as well.

Theorem 4.3. *Consider the coordination laws in (3.23), (3.24) and (4.8), where $v(t)$ is parameterized as (4.1) in which $\phi^j(t)$, $\dot{\phi}^j(t)$, $j = 1, \cdots, r$ are continuous and uniformly bounded. With u_i defined in (3.68), and $\mathscr{H}_i$, $i = 1, \cdots, N$, and ψ_k, $k = 1, \cdots, \ell$ designed as in (2.11)-(2.15) and (2.27)-(2.31), all trajectories $(z(t), \xi(t), \hat{\theta}(t))$ starting in $\mathscr{G} \times \mathbb{R}^{pr(N-1)}$ are bounded and converge to the set*

$$\mathscr{E}_p^* = \left\{ (z, \xi, \hat{\theta}) | \xi = 0, (D \otimes I_p)\psi(z) = 0, z \in \mathscr{R}(D^T \otimes I_p), \hat{v}_i(t) = v(t) \right\}, \quad (4.40)$$

where $\hat{v}_i(t)$ is defined in (4.4) and $\mathscr{G}$ is as in (2.37). □

The closed-loop structure of the augmented adaptive design is given in Fig. 4.2. Recall from Property 1.4 that $\dot{x}^T (L^v \otimes I_p)\dot{x} = \frac{1}{2}\dot{x}^T (L^v_{\text{sym}} \otimes I_p)\dot{x}$, which is nonnegative since G^v is strongly connected and balanced. Thus, the static block L^v_{sym} in Fig. 4.2 is passive and the feedforward path from $\dot{x}$ to $-u$ is also passive. As the passivity of the feedback path is already established in Theorem 4.1, we conclude the closed-loop stability of the system in Fig. 4.2.

Proof. Note that (3.68) can be rewritten in the compact form (3.69). To prove the stability of the closed-loop system described by the adaptive design (2.11), (3.55), (3.69) and (4.11), we take the same Lyapunov function as in (4.17) and from (2.40), (3.70), (4.16) and (3.69), compute its time derivative as

$$\dot{V} = -\sum_{i \in \mathscr{I}} W_i(\xi_i) - \sum_{i \notin \mathscr{I}} u_i^T y_i - (y + \tilde{v})^T (L^v \otimes I_p)(y + \tilde{v}) \leq 0 \quad (4.41)$$

which implies stability and boundedness of $(z(t), \xi(t), \tilde{\theta}(t))$. Using Theorem B.5, we further conclude that $\xi_i \to 0$, $\forall i \in \mathscr{I}$, $u_i \to 0$, $\forall i \notin \mathscr{I}$ and $(y + \tilde{v})^T (L^v \otimes I_p)(y + \tilde{v}) \to 0$. For dynamic block $\mathscr{H}_i$, it follows from $\xi_i \to 0$ and (2.11) that $y_i \to 0$. For static block $\mathscr{H}_i$, $u_i \to 0$ implies $y_i = h_i(u_i) \to 0$. Thus, $y \to 0$. Recall from (1.20) that $(y + \tilde{v})^T (L^v \otimes I_p)(y + \tilde{v})$ is zero only when $(y + \tilde{v})^T (L^v_{\text{sym}})(y + \tilde{v})$ is zero. Since the graph G^v is strongly connected, the graph corresponding to L^v_{sym} is connected. Therefore, $(y + \tilde{v})^T (L^v \otimes I_p)(y + \tilde{v}) = 0$ implies $y + \tilde{v} = 1_N \otimes c$, where $c \in \mathbb{R}^p$. We

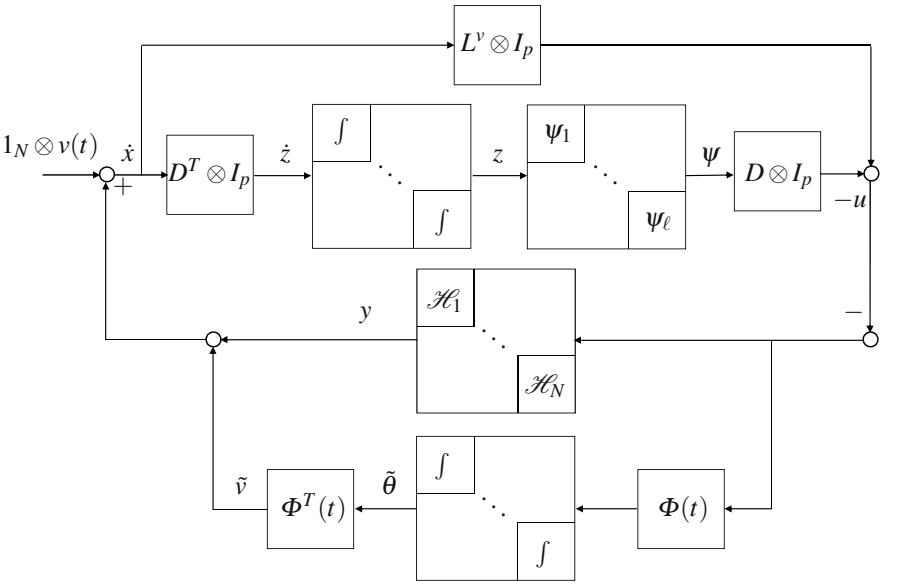

Fig. 4.2 The closed-loop structure of the augmented adaptive design. The property of L^v in (1.20) renders the passivity of the top loop. The closed-loop stability follows from the interconnection of two passive feedforward paths and two passive feedback paths.

conclude from $\tilde{v}_1 \equiv 0$ and $y_1 \to 0$ that $|y+\tilde{v}| \to 0$. Since $y \to 0$, it follows that $\tilde{v} \to 0$, which implies from (4.14) that tracking of $v(t)$ is achieved.

We next show $u \to 0$. To this end we note that

$$\ddot{\xi}_i = \frac{\partial f_i}{\partial u_i}\dot{u}_i + \frac{\partial f_i}{\partial \xi_i}\dot{\xi}_i \tag{4.42}$$

is continuous and uniformly bounded because $\dot{u}$ and $\dot{\xi}$ are continuous functions of the bounded signals $(z(t), \xi(t), \tilde{\theta}(t), \Phi(t), \dot{\Phi}(t))$ and because $f_i(\cdot,\cdot)$ is C^1. Since $\xi_i \to 0$ and $\ddot{\xi}_i$ is continuous and bounded, it follows from Theorem B.4 that $\dot{\xi}_i \to 0$, which, from (2.11) and (2.12), guarantees $u_i \to 0$. Since $|y+\tilde{v}| \to 0$, we conclude from (3.69) that $(D \otimes I_p)\psi(z) \to 0$. □

The main difference of Theorem 4.3 from Theorem 4.2 is that it achieves reference velocity tracking directly while Theorem 4.2 establishes tracking by first achieving parameter convergence. Parameter convergence is sufficient but not necessary for velocity tracking (compare (4.1) and (4.4)). We next show that velocity tracking implies parameter convergence $\hat{\theta}_i \to \theta$ when the regressor $\Phi(t)$ satisfies the PE condition in (4.23). We need the following lemma.

Lemma 4.1. *Let*

$$\dot{X} = f(X,t), \tag{4.43}$$

where $X \in \mathbb{R}^n$ and $f(X,t) : \mathbb{R}^n \times \mathbb{R}_{\geq 0} \to \mathbb{R}^n$. If all trajectories $X(t)$ satisfy $f(X(t),t) \to 0$ and $\Omega(t)^T X(t) \to 0$, where $\Omega(t) \in \mathbb{R}^n$ is bounded and satisfies the PE property in (4.23), then $X(t) \to 0$. □

Proof. We rewrite (4.43) as

$$\dot{X} = -\Omega(t)\Omega(t)^T X + \zeta(t) \tag{4.44}$$

where $\zeta(t) := \Omega(t)\Omega(t)^T X + f(X,t)$, and note that $\zeta(t) \to 0$ since $\Omega(t)^T X$ and $f(X,t)$ both converge to zero and since $\Omega(t)$ is bounded. Solving for X from the linear time-varying model (4.44), we obtain

$$X(t) = \Xi(t,t_0)X(t_0) + \int_{t_0}^{t} \Xi(t,\tau)\zeta(\tau)d\tau \tag{4.45}$$

where $\Xi(t,t_0)$ is the state transition matrix. Because $\Omega(t)$ is PE and because $\zeta(t) \to 0$ as $t \to \infty$, it follows from standard results in adaptive control (e.g., [62, 136]) that $X(t) \to 0$. □

We now combine Theorem 4.3 and Lemma 4.1 to prove parameter convergence:

Corollary 4.1. *Suppose all conditions of Theorem 4.3 hold. If, in addition, $\Phi(t)$ satisfies (4.23), then $\hat{\theta}_i \to \theta$.* □

Proof. We establish $\hat{\theta}_i \to \theta$ by using the PE property (4.23) and Lemma 4.1 to prove that $|\tilde{v}| \to 0$ implies $\tilde{\theta}_i \to 0$, that is $\hat{\theta}_i \to \theta$.

We note from Theorem 4.3 that

$$\tilde{v} = (I_N \otimes \Phi^T(t) \otimes I_p)\tilde{\theta} \to 0 \tag{4.46}$$

and that

$$\dot{\tilde{\theta}}_i = \Lambda_i(\Phi(t) \otimes I_p)u_i \to 0 \tag{4.47}$$

since $u_i \to 0$. Because the signal $\Phi^T(t)$ is PE, it follows from Lemma 4.1 that $\tilde{\theta}_i \to 0$, which proves the parameter convergence $\hat{\theta}_i \to \theta$. □

Example 4.2. To illustrate the parameter convergence, we simulate the example in Section 3.5.1. We take

$$v(t) = ([\sin(t)\ \cos(t)] \otimes I_2) \begin{bmatrix} \theta^1 \\ \theta^2 \end{bmatrix} \tag{4.48}$$

where $\theta^1 = [-\frac{\sqrt{3}}{3}\ 0]^T$ and $\theta^2 = [0\ \frac{\sqrt{3}}{3}]^T$. This $v(t)$ is the same as in Section 3.4.2. The estimate $\hat{v}_i(t)$ in (3.64) is obtained from (4.4) with $\Phi(t) = [\sin(t)\ \cos(t)]^T$ and $\hat{\theta}_i = [(\hat{\theta}_i^1)^T\ (\hat{\theta}_i^2)^T]^T$ updated by (4.8).

The initial conditions of $x_i(0)$, $i = 1,2,3$, $\xi_1(0)$, and $\hat{\xi}_i(0)$, $i = 2,3$ are the same as in Section 3.4.2. The initial estimates are set to $\hat{\theta}_2(0) = [\frac{\sqrt{3}}{6}\ -\frac{1}{2}\ -\frac{1}{2}\ -\frac{\sqrt{3}}{6}]^T$ and $\hat{\theta}_3(0) = [\frac{\sqrt{3}}{6}\ \frac{1}{2}\ \frac{1}{2}\ -\frac{\sqrt{3}}{6}]^T$ such that the group exhibits the same motion as in Fig. 3.4(b) if (2.23) is used in (4.8).

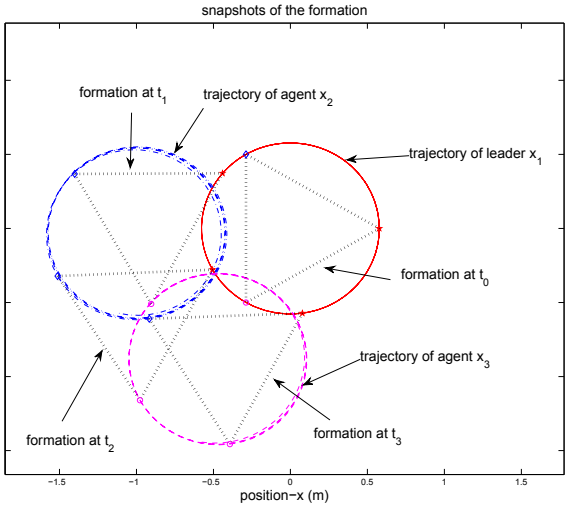

Fig. 4.3 The augmented adaptive design recovers the convergence properties of the nonadaptive design. [13]. Reprinted with Permission. Copyright Elsevier 2009.

When the augmented feedback (3.68) is employed in (4.8), Fig. 4.3 shows the snapshots of the formation. The group now exhibits a translational motion with x_1 circling around the origin, which means that the nonadaptive results are fully recovered. In addition, because $\Phi(t)$ is PE, parameter convergence is achieved as shown in Fig. 4.4. In this simulation, the graphs G and G^v are chosen the same as in Section 3.5.1. □

4.5 Application to Gradient Climbing in Formation

In this section, we apply the adaptive design result to a gradient climbing problem, where the group leader performs extremum seeking for the field minima or maxima, while the other agents maintain a desired formation with respect to the leader. Keeping a group formation during the gradient climbing may be desirable for reliable inter-vehicle communication/sensing, drag reduction, safety in adversarial environments, etc.

To achieve gradient climbing in a field distribution, the leader takes a discrete-time, optimization based extremum seeking approach. This extremum-seeking approach, illustrated in Fig. 4.5, generates finite-difference approximations for the gra-

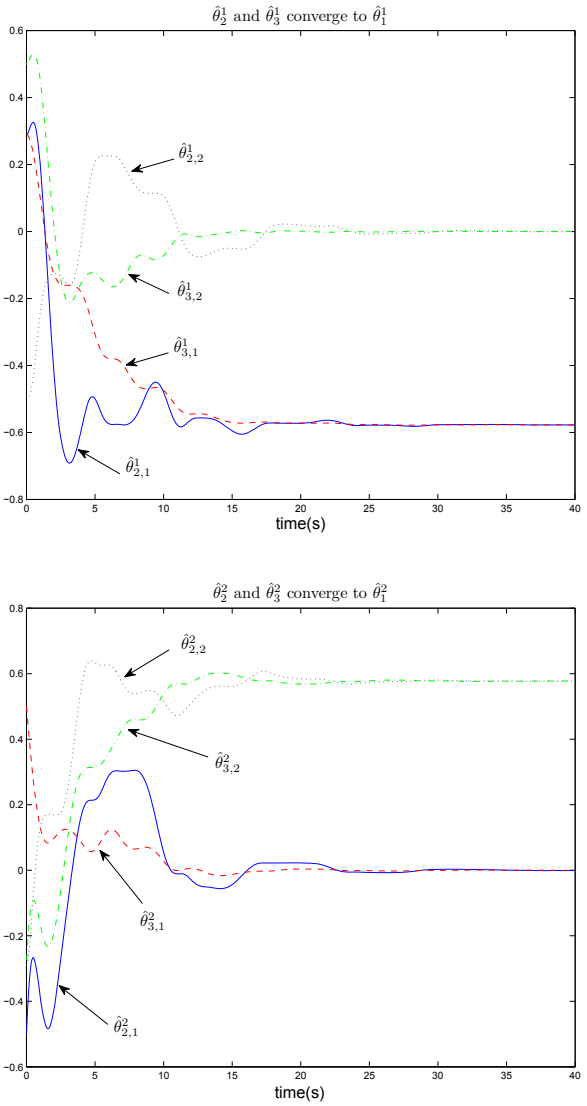

Fig. 4.4 Parameter convergence with the augmented adaptive design. $\hat{\theta}_2^1$ and $\hat{\theta}_3^1$ converge to $\theta^1 = [-\frac{\sqrt{3}}{3}\ 0]^T$ while $\hat{\theta}_2^2$ and $\hat{\theta}_3^2$ converge to $\theta^2 = [0\ \frac{\sqrt{3}}{3}]^T$. [13]. Reprinted with Permission. Copyright Elsevier 2009.

dient and the Hessian of the field, by "dithering" sensor positions. The advantage of this local approximation is that only the leader needs sensing capabilities, and communication of sensed variables and geographic proximity of sensors are not necessary for generating approximate gradients.

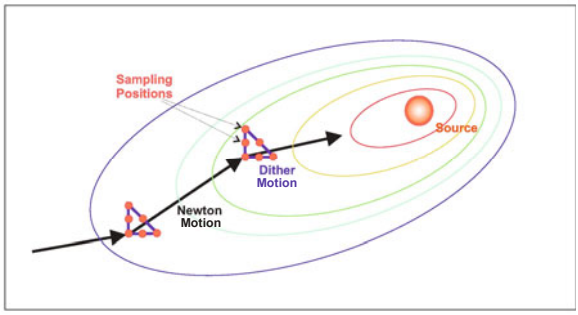

Fig. 4.5 Gradient climbing by extremum seeking. Arrows represent the Newton motion, while triangular paths are the dither motion with the samples taken at positions marked by dots. The dither motion has three segments: Along horizontal axis from left to right, along the diagonal from right to left and along vertical axis from top to bottom. The directions of these three segments are denoted by $[1,0]$, $[-1,1]$, $[0,-1]$.

After the dither motion, the leader calculates a Newton direction towards the field extremum. Thus, the group reference velocity $v(t)$ is determined autonomously by the leader, in the form of segments $v_k(t)$, $t \in [t_k, t_{k+1}]$, that are updated in every iteration k according to the next Newton direction. Since $v(t)$ is not available to the other agents, they need to estimate this $v(t)$ information to achieve a successful gradient climbing in the desired formation.

We let the leader parameterize its reference velocity as in (4.1) and apply the *basic* adaptive design in this chapter to ensure a desired group formation. During the dither motion of the leader, the other agents may turn off the velocity adaptation design so that they do not respond to the dither motion of the leader. Even if the adaptation is not turned off, we show with simulation results that if the Newton motion lasts sufficiently long, the followers respond only to the Newton motion while filtering out the dither component.

4.5.1 Reference Velocity Assignment by the Leader

In this section, we present the extremum seeking scheme performed by the leader. The analysis of the motion of the group will be pursued in Section 4.5.2. The goal in extremum-seeking based gradient climbing is to search for and move towards the maximum of a field distribution with an unknown functional form. The leader has access only to the scalar field measurements, and constructs the approximate gradient and Hessian information of the field by finite-difference methods to compute a Newton direction. It then assigns an appropriate velocity along the computed Newton direction. It is important to note that this scheme locates the maxima without position measurements.

We first review basic optimization tools that are instrumental in the extremum seeking design. We assume that the field has a spatial distribution characterized by a twice continuously differentiable function $F(x) : \mathbb{R}^2 \to \mathbb{R}$ that has a unique maximum at $x = x^*$. Note that we restrict our attention to fields only in $\mathbb{R}^2$, however, the results can be extended to $\mathbb{R}^3$ as well by employing appropriate finite-difference approximations. Also note that if the function $F(x)$ has multiple maxima, then the results can be modified to prove regional convergence to the local maximum. Because only field measurements are available to the leader, we approximate the gradient and Hessian of $F(x)$ by one-sided finite-difference gradient, G_k,

$$\nabla F(x_k) \approx G_k[i] := \frac{F(x_k + h_k e_i) - F(x_k)}{h_k} \tag{4.49}$$

and Hessian, H_k,

$$\begin{aligned} \nabla^2 F(x_k) \approx H_k[i,j] := \frac{1}{h_k^2}\Big[& F(x_k) + F(x_k + h_k e_i + h_k e_j) \\ & - F(x_k + h_k e_i) - F(x_k + h_k e_j)\Big] \end{aligned} \tag{4.50}$$

where h_k denotes the finite-difference "dither" size, and e_i is the i^{th} unit vector. For an easier implementation, steepest descent may be preferable over Newton's Method; however, it is slower and does not provide a concrete convergence proof with nonvanishing step-size. We denote by $\mathbf{B}(\bar{x}, a)$ the ball of radius a centered at $\bar{x}$, i.e., $\mathbf{B}(\bar{x}, a) := \{x \mid |x - \bar{x}| \leq a\}$. The lemma below states that for sufficiently small dither size h_k, and for small initial error $|x_0 - x^*|$, finite-difference based Newton's Method locally converges to an $O(h)$-neighborhood of x^*. The proof follows from standard arguments in unconstrained optimization theory, and is given in Appendix A.3.

Lemma 4.2. *Let $F(x) : \mathbb{R}^2 \to \mathbb{R}$ be twice continuously differentiable in an open convex set $\mathscr{D} \in \mathbb{R}^2$. Assume there exists a unique $x^* \in \mathbb{R}^2$, $r > 0$ and $\beta > 0$ such that $\mathbf{B}(x^*, r) \in \mathscr{D}$, $\nabla F(x^*) = 0$, $\nabla^2 F(x^*)^{-1}$ exists with $||\nabla^2 F(x^*)^{-1}|| \leq \beta$, and $\nabla F(x)$ and $\nabla^2 F(x)$ are Lipschitz continuous. Then there exist $\varepsilon > 0$ and $\bar{h} > 0$, such that for all initial conditions $x_0 \in \mathbf{B}(x^*, \varepsilon)$, and dither size $h_k < \bar{h}$ the sequence $\{x_k\}_{k=0}^{k=\infty}$ generated by*

$$x_{k+1} = x_k + H_k^{-1} G_k, \quad k = 0, 1, \cdots \tag{4.51}$$

where G_k and H_k are as in (4.49)-(4.50) converges to an $O(\bar{h})$ neighborhood of x^* q-linearly. □

We next introduce the Newton's Method-based gradient climbing scheme that the leader implements to locate the maximum of a field. We consider the agent model in (2.16) and the control design (2.17). We assume that the leader, say agent 1, does not receive external feedback u_i from other members of the group, hence $u_1 \equiv 0$. Recall that (2.16) and (2.17) can be transformed to (2.19) and (2.20). We then assume $\xi_1(0) = 0$, which implies from (2.19) and (2.20) that

$$\dot{x}_1 = v(t). \tag{4.52}$$

Note that if $\xi_1(0) \neq 0$, we can apply the velocity input $\bar{v}(t) = -\xi_1 + v(t)$ to the leader, and recover (4.52).

We use Newton's Method to determine the next position for the leader, and set the reference velocity $v(t)$ to steer the leader to that position. As illustrated in Fig. 4.5, in the kth extremum-seeking iteration, the leader first moves in $[1,\ 0]$, $[-1,\ 1]$, and $[0,\ -1]$ directions rapidly to take samples of the field $F(x)$ and computes the approximate gradient G_k and the Hessian H_k as in (4.49)-(4.50), and then moves in the approximate Newton direction $l_k = H_k^{-1} G_k$, and arrives at $x_{k+1} = x_k + l_k$.

To prepare for an adaptive reference velocity estimation by the followers, we parameterize $v(t)$ in a form similar to (4.1). For each motion segment we let the reference velocity have a fixed sinusoidal amplitude profile, with endpoints at zero, and change its direction between successive segments. We denote by $v_{[i,j]}$ and v_N the dither velocity in the $[i, j]$ direction, where $[i, j] \in \{[1,0],[-1,1],[0,-1]\}$, and the Newton velocity in l_k direction, respectively. Let t_d be the duration of each dither motion segment, and T be that of the Newton motion. Therefore one iteration of the extremum seeking scheme takes $\Delta := 3t_d + T$ seconds. During each extremum seeking iteration, the leader switches its velocity as

$$\dot{x}_1 = v(t) := \begin{cases} v_{[1,0]}(t), & \text{if } t_k \le t < t_k + t_d, \\ v_{[-1,1]}(t), & \text{if } t_k + t_d \le t < t_k + 2t_d, \\ v_{[0,-1]}(t), & \text{if } t_k + 2t_d \le t < t_k + 3t_d, \\ v_N(t), & \text{if } t_k + 3t_d \le t < t_{k+1}, \end{cases} \tag{4.53}$$

where

$$t_k := k\Delta, \quad k = 0, 1, 2, \cdots, \tag{4.54}$$

and $v_{[1,0]}$, $v_{[-1,1]}$, $v_{[0,-1]}$ and v_N are defined as:

$$v_{[1,0]}(t) := \frac{2h_k}{t_d} \begin{bmatrix} 1 \\ 0 \end{bmatrix} \left(1 - \cos(\frac{2\pi}{t_d}(t - t_k))\right) \tag{4.55}$$

$$v_{[-1,1]}(t) := \frac{2h_k}{t_d} \begin{bmatrix} -1 \\ 1 \end{bmatrix} \left(1 - \cos(\frac{2\pi}{t_d}(t - t_k - t_d))\right) \tag{4.56}$$

$$v_{[0,-1]}(t) := \frac{2h_k}{t_d} \begin{bmatrix} 0 \\ -1 \end{bmatrix} \left(1 - \cos(\frac{2\pi}{t_d}(t - t_k - 2t_d))\right) \tag{4.57}$$

$$v_N(t) := \frac{l_k}{T} \left(1 - \cos(\frac{2\pi}{T}(t - t_k - 3t_d))\right). \tag{4.58}$$

The reference velocity $v(t)$ in (4.53) and its derivative $\dot{v}(t)$ are continuous, and $(v(t), \dot{v}(t))|_{t \in \{t_k + nt_d,\ t_{k+1}\}} = (0,0)$, $n = 0,1,2,3$. Note that other continuous velocity profiles that vanish at $t \in \{t_k + nt_d,\ t_{k+1}\}$, $n = 0,1,2,3$, along with their derivatives, are also applicable. The velocities in (4.55)-(4.58), when switched according to (4.53), achieve one iteration of extremum-seeing motion by driving the leader first to the appropriate "dither" positions and then to the next "Newton" position

x_{k+1}. Theorem 4.4 below proves that the extremum seeking scheme converges to an $O(\bar{h})$ neighborhood of the maximum x^*, when $h_k \leq \bar{h}$ is as in Lemma 4.2, and $|x(0)-x^*|$ is sufficiently small.

Theorem 4.4. *Let the field distribution $F(x)$ be twice continuously differentiable with a unique maximum at position $x = x^* \in \mathbb{R}^2$. Suppose the assumptions in Lemma 4.2 hold and $\bar{h}$ be as defined therein. Then the Newton-based extremum seeking scheme applied to the vehicle model in (4.53) with velocity profiles (4.55)-(4.58) drives the vehicle to the $O(\bar{h})$ neighborhood of x^*, provided that $h_k \leq \bar{h}$ and $|x(0) - x^*|$ is sufficiently small.* □

Proof. We show that the reference velocity profiles given in (4.53) first drive the leader in the appropriate dither directions, and then along the Newton direction. Consider $v_{[1,0]}$ which drives the leader in horizontal position, i.e., along the vector $[1,0]$. At time t_k, let the position of the leader be $x_1(t_k) = [x_1^1(t_k), x_1^2(t_k)]^T \in \mathbb{R}^2$. Then at time $t_k + t_d/2$ its position is:

$$\begin{aligned} x_1(t_k + \frac{t_d}{2}) &= x_1(t_k) + \int_{t_k}^{t_k+t_d/2} v_{[1,0]}(t)dt \\ &= x_1(t_k) + \frac{2h_k}{t_d}\begin{bmatrix}1\\0\end{bmatrix}\int_{t_k}^{t_k+t_d/2}(1-\cos(\frac{2\pi}{t_d}(t-t_k)))dt \\ &= x_1(t_k) + \frac{2h_k}{t_d}\begin{bmatrix}1\\0\end{bmatrix}\left[t - \frac{t_d}{2\pi}\sin(\frac{2\pi}{t_d}(t-t_k))\right]\Big|_{t_k}^{t_k+t_d/2} \\ &= x_1(t_k) + h_k\begin{bmatrix}1\\0\end{bmatrix} = \begin{bmatrix}x^1(t_k)+h_k\\ x^2(t_k)\end{bmatrix}. \end{aligned} \tag{4.59}$$

Likewise,

$$\begin{aligned} x_1(t_k + t_d) &= x_1(t_k + t_d/2) + \int_{t_k+t_d/2}^{t_k+t_d} v_{[1,0]}(t)dt \\ &= x_1(t_k + t_d/2) + h_k\begin{bmatrix}1\\0\end{bmatrix} = \begin{bmatrix}x^1(t_k)+2h_k\\ x^2(t_k)\end{bmatrix}. \end{aligned} \tag{4.60}$$

Similar calculations show that $v_{[-1,1]}$ and $v_{[0,-1]}$ achieve the desired dither motions as well. Note that after the third dither motion $v_{[0,-1]}$ the leader will be back at position $x_1(t_k + 3t_d) = x_1(t_k)$. Then, applying the "Newton" velocity v_N after this point for T seconds drives the leader to

$$\begin{aligned} x_1(t_k + \Delta) &= x_1(t_k) + l_k\frac{1}{T}\int_{t_k+3t_d}^{t_k+3t_d+T}(1-\cos(\frac{2\pi}{T}(t-t_k-3t_d)))dt \\ &= x_1(t_k) + l_k = x_1(t_{k+1}). \end{aligned} \tag{4.61}$$

Therefore, by switching the velocities as in (4.53) the leader visits all dither positions and moves to the next Newton position. The convergence result follows from Lemma 4.2. □

4.5.2 Gradient Climbing in Formation

We have shown that using the switching strategy in (4.53) with the reference velocity $v(t)$ parameterized as in (4.55)-(4.58), the leader locates the extrema of the field. We next investigate how to design the motion of the other agents to achieve gradient climbing in a desired formation.

As discussed in Section 2.6, we may pursue the position-based or distance-based formation control formulation. In either formulation, we note that the other agents do not have the knowledge of the reference velocity $v(t)$ which changes after each iteration of extremum seeking. Therefore, the adaptive designs in Chapter 3 and this chapter can be applied to estimate the $v(t)$ information. Since (4.55)-(4.58) are already parameterized as a product of a vector and a time-varying basis function, we will take the parameterization approach in this chapter. Then the dynamics of agent i, $i = 2, \cdots, N$ are given by the basic adaptive design (3.24), (2.11), (4.4), and (4.8), where we assume that u_i has already been designed according to the position-based or distance-based formation control formulation. Following (4.53), we obtain the basis function $\Phi(t) \in \mathbb{R}$ and the constant parameter $\theta \in \mathbb{R}^2$ in (4.1) as

$$\Phi(t) := \begin{cases} \left(1-\cos(\frac{2\pi}{t_d}(t-t_k))\right), & \text{if } t_k \le t < t_k + t_d, \\ \left(1-\cos(\frac{2\pi}{t_d}(t-t_k-t_d))\right), & \text{if } t_k + t_d \le t < t_k + 2t_d, \\ \left(1-\cos(\frac{2\pi}{t_d}(t-t_k-2t_d))\right), & \text{if } t_k + 2t_d \le t < t_k + 3t_d, \\ \left(1-\cos(\frac{2\pi}{T}(t-t_k-3t_d))\right), & \text{if } t_k + 3t_d \le t < t_{k+1}, \end{cases} \tag{4.62}$$

and

$$\theta := \begin{cases} \frac{2h_k}{t_d}\begin{bmatrix} 1 \\ 0 \end{bmatrix}, & \text{if } t_k \le t < t_k + t_d, \\ \frac{2h_k}{t_d}\begin{bmatrix} -1 \\ 1 \end{bmatrix}, & \text{if } t_k + t_d \le t < t_k + 2t_d, \\ \frac{2h_k}{t_d}\begin{bmatrix} 0 \\ -1 \end{bmatrix}, & \text{if } t_k + 2t_d \le t < t_k + 3t_d, \\ \frac{l_k}{T}, & \text{if } t_k + 3t_d \le t < t_{k+1}. \end{cases} \tag{4.63}$$

In each motion segment, agent i employs the basic adaptive design in Section 4.2 to estimate θ by $\hat{\theta}_i$ and reconstruct the desired formation.

If t_d and T are sufficiently large, the result in Theorem 4.1 implies that the desired formation is ensured during each motion segment. This means that the agents will follow both the dither and the Newton motions of the leader. However, if only the leader has the sensing ability, it may be desired that the other agents respond only to the Newton motion. This can be achieved by simply turning off the adaptation during the dither motion periods. Even if adaptation is not turned off, the other agents detect only the Newton motion if T is sufficiently larger than t_d. To see this, we note from (4.53) that the average velocity of $v(t)$ within one extremum seeking

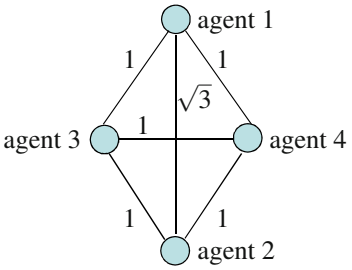

Fig. 4.6 The desired formation of four agents in the gradient climbing. The number indicates the desired length of each link.

iteration is given by

$$v_{av} := \frac{1}{\Delta}\int_{t_k}^{t_k+\Delta} v(t)dt = \frac{1}{\Delta}l_k. \tag{4.64}$$

Then if T is sufficiently large, $\Delta \approx T$ and thus $v_{av} \approx \frac{1}{T}l_k$, which is indeed the average of $v_N(t)$ in (4.58) in one Newton motion period. This implies that for sufficiently large T, the dither motion is averaged out. Thus, we can choose a sufficiently large T to ensure that the other agents follow only the Newton motion within each extremum-seeking iteration. In fact, for large T, one can further reveal a time-scale separation behavior in the group motion and show that the convergence to the desired formation is achieved in the fast time scale, while the Newton motion is performed in the slow time-scale. We refer interested readers to [18] for further details.

4.5.3 Simulation Results

We simulate the gradient climbing of four agents modeled by (2.16) with $m_i = 1$. We consider the distance-based formation control in Section 2.7.1. The desired formation is a rhombus formation shown in Fig. 4.6. Note from Example 2.5 that to ensure an unambiguous desired formation of four agents, we need to specify the desired relative distances between every two agents. According to Fig. 4.6, we define $z_1 = x_1 - x_2$ and set its desired distance as $d_1 = \sqrt{3}$. For the other z_k's, $k = 2, \cdots, 6$, their desired distances are $d_k = 1$. Given d_k's, the nonlinearity $\psi_k(z_k)$ can be designed according to (2.83)-(2.87). For the simulations we take $\sigma_1(s) = \ln(s/\sqrt{3})$ and $\sigma_k(s) = \ln(s)$, $k = 2, \cdots, 6$.

We let the field distribution be

$$F(x,y) = e^{-0.1e^{0.1x}(1.1x-5)^2 - 0.2e^{0.1y}(0.8y-4)^2},$$

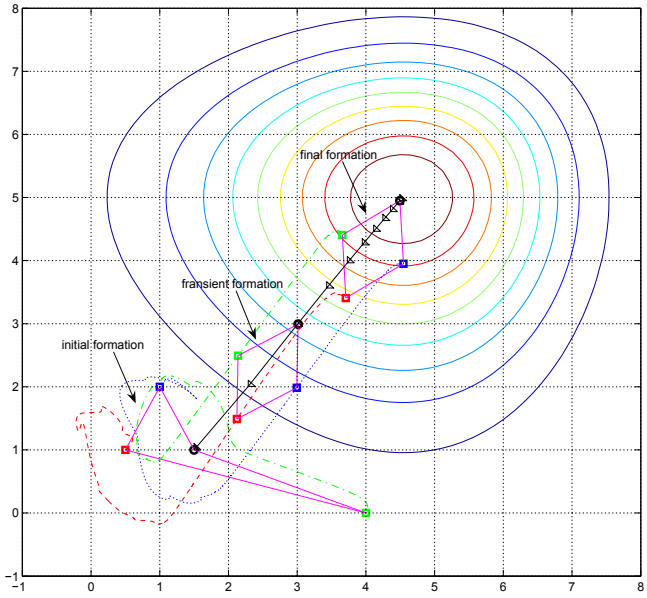

Fig. 4.7 Gradient climbing by Newton-based extremum seeking with $T = 18.5$ sec, $t_d = 0.5$ sec, and $h_k = 0.05$. Solid line represents the leader's trajectory, while dashed line, dash-dot line, and dots are the followers'. After an initial transient agents follow the leader's Newton motion in a rhombus formation, and average out the fast dither perturbations.

which has a global maximum at $x = [4.55, 5]^T$. We fix $\Delta = 20$ sec and $h_k = 0.05$, and pick $t_d = 0.5$ sec and $T = 18.5$ sec for the first simulation. We run the system (4.52) and (3.24), where the leader determines its velocity by extremum seeking as in (4.53) and (4.55)-(4.58) and the other agents estimate $v(t)$ by (4.4) with $\Phi(t)$ in (4.62). Fig. 4.7 shows that after an initial transient, agents follow the leader's Newton motion in a rhombus formation, and average out the fast dither perturbations, while the leader locates the maxima of the field. In the second simulation, we perform the dither motion at a slower speed with $t_d = 4$ sec, $T = 8$ sec. In this case, the agents in Fig. 4.8 fail to average out the dither motion, and follow a jittering trajectory.

4.6 Summary

In Chapters 3 and 4, we studied a group coordination problem where the reference velocity is available to only one agent while the others estimate this information with adaptive designs. We presented two approaches to the adaptive designs. The first approach assumes a constant or a periodic reference velocity while the second approach parameterizes the reference velocity as linear combinations of known time-varying basis functions with unknown coefficients. For each approach, we first

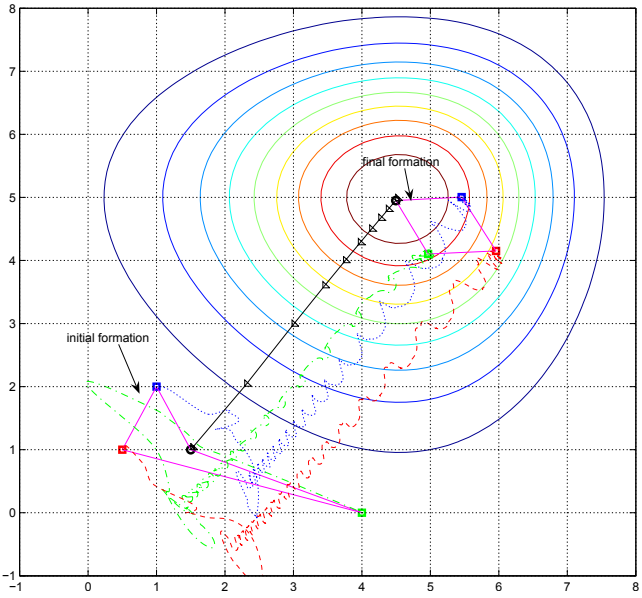

Fig. 4.8 Gradient climbing by Newton-based extremum seeking with $T = 8$ sec, $t_d = 4$ sec, and $h_k = 0.05$. Solid line represents the leader's trajectory, while dashed line, dash-dot line, and dots are the followers'. The agents fail to average out the dither motion, and follow a jittering trajectory.

proposed a basic adaptive design that guarantees objective A2. We showed that tracking of the reference velocity is recovered for some special cases including the agreement problem. We presented an example which shows that the estimates of the reference velocity may fail to converge to a time-varying reference velocity. For each approach, we then proposed an augmented adaptive redesign that employs relative velocity feedback in addition to relative position feedback and achieves tracking of the reference velocity.

We next applied the basic adaptive design in this chapter to an extremum seeking example, where the leader autonomously determines the Newton direction based on samples of a field distribution and parameterizes the group reference velocity according to the Newton direction. The other agents then estimate the reference velocity using the parameterization approach. In the simulation, we showed that if the Newton motion lasts sufficiently long within each extremum seeking period, the desired formation is reconstructed during gradient climbing.

4.7 Notes

• The extremum seeking results in this chapter are based on [18].

• The extremum seeking approach in this chapter relies on nonlinear optimization techniques to estimate the gradient in discrete time. An alternative approach in extremum seeking is to probe the system with sinusoidal inputs, and to make an online estimation of the gradient of the output relative to these inputs [151, 7].
• To enhance robustness to noise and input disturbance, existing modifications of adaptive design, such as σ-leakage modification [62], can be applied to the adaptive designs in Chapter 3 and this chapter.